Three-dimensional Particle Acceleration in Electromagnetic Cylinder and Torus

Koichi Noguchi and Edison Liang

Rice University, Houston, TX 77005-1892

(Dated: September 11, 2006)

Abstract

Particle acceleration via Poynting vector with toroidal magnetic field is studied in 3D PIC simulation of electron-positron plasma. We choose two different initial magnetic field configurations to compare how the particle acceleration is affected by the expansion of electromagnetic wave. In the cylindrical case, the electromagnetic field strength decays as $(ct)^{-2}$, and particles are accelerated in the radial direction as well as the axial direction. Rayleigh-Taylor instability is also observed at the center of the cylinder. In the torus case, the field strength decays as $(ct)^{-3}$, making the acceleration less efficient. Particles accelerated in the axial direction by $E \times B$ force creates strong charge separation.

Keywords: gamma rays:bursts—MHD—methods:numerical—relativity

I. INTRODUCTION

One of the most famous models to produce a GRB and large explosion energy from the death of a massive star is the collapsar model [6, 11]. When a massive star is collapsing to a black hole, it accretes envelope matter at a very high rate. Woosley pointed out that neutrinos should be emitted from the innermost region of the accretion disk through the electron-positron capture and electron-positron pair annihilation [2, 6]. A strong jet with a large explosion energy on the order of $\sim 10^{52}$ ergs, is generated from the polar region by the pair-annihilation of neutrinos, and the shock wave propagates through a channel created inside of the stellar envelope. Two-dimensional relativistic hydrodynamic simulations with nucleosynthesis [6–9] confirms the formation and propagation of jets inside of the stellar envelope.

Poynting flux acceleration (PFA) may be launched when the magnetic jet head or the magnetar stripe wind emerge from the stellar envelope surface due to the sudden deconfinement of the magnetic field and embedded electron-positron plasma. When the electron-positron plasma jet is emerged out from the envelope, electromagnetic wave expands into ambient medium with particles accelerated by the PFA [4, 10]. Since magnetic fields are connected to the accretion disk associated with the collapsar, the emerged jet is collimated and creates a magnetic tower [5]. Three-dimensional magnetohydrodynamic global simulations of a central black hole associated with low magnetized accretion disk [3] shows that vertically inflating toroidal fields supports the magnetic jet collimation.

In this article we present 3D PIC simulations of particle acceleration driven by PFA with two different initial magnetic field configurations. In the first model, initial toroidal magnetic field and particle distributions are a decreasing function of radius, and have infinite length in the axial direction. In the second model, magnetic field and particles are distributed as a radially decreasing function as the same as the first model, but has a finite length in the axial direction. The first model represents the particle acceleration in the magnetic tower, and the second represents the magnetic jet head emerged from the stellar envelope. Hereafter we call the first model as the cylindrical case and the second as the torus case, respectively.

II. INITIAL SETUP OF THE SIMULATION

We use the 3D explicit PIC simulation scheme based on the Yee algorithm[12]. Spatial grids for the fields are uniform in all directions, $\Delta x = \Delta y = \Delta z = c/\omega_{pe}$, where ω_{pe} is the electron plasma frequency. We employ 128^3 cells with triply periodic boundary conditions. In the simulation, the origin is located at the center, and x direction corresponds to the axis of the magnetic cylinder and torus.

For both the cylindrical and torus cases, the radial profiles of initial magnetic field and particle density are the same. In order to make the magnetic field satisfy $\nabla \cdot \boldsymbol{B} = 0$, the initial magnetic field profile has toroidal component only, which is given as

$$B_\phi = \begin{cases} B_0 r/(2\Delta x), & 0 \le r < 2\Delta x \\ 2B_0 \Delta x/r, & 2\Delta x \le r \le 8\Delta x \end{cases} . \tag{1}$$

We note that the radial profile of B_ϕ corresponds to the profile around cylindrical infinite current column with $j = cB_0/4\pi r (r < 2\pi\Delta x)$. For simplicity and self-consistency, we assume no initial electric field and current. Electric field and current are self-induced by magnetic field and particle motion associated with it. In magnetic-tower scenario, magnetic field near the tip of a jet is almost purely toroidal, and plasma motion is driven by magnetic field expansion.

The density profile is given as

$$\rho = \begin{cases} \rho_0 r/(2\Delta x), & 0 \le r < 2\Delta x \\ 2\Delta x \rho_0/r, & 2\Delta x \le r \le 5\Delta x \end{cases} . \tag{2}$$

Here, ρ_0 is calculated by assuming $\omega_{pe}/\Omega_{ce} = 0.1$, where Ω_{ce} is the electron cyclotron frequency.

The initial temperature of plasma is a spatially uniform Maxwellian $k_B T_e = k_B T_p = 100$eV, where T_e and T_p are the electron and positron temperature, respectively. We note that we use c/ω_{pe} instead of electron Debye length as a unit scale in the simulations, because EM field expands with the speed of light rather than the thermal speed.

In the cylindrical case, B_ϕ and ρ are uniform in the z direction. In the torus case, however, both B_ϕ and ρ vanishes for $z < -2c/\omega_{pe}$ and $z > 2c/\omega_{pe}$ in order to simulate the magnetic jet head. Initial temperature is assumed to be uniform Maxwellian with $k_B T_e = k_B T_{p,i} = 100$eV.

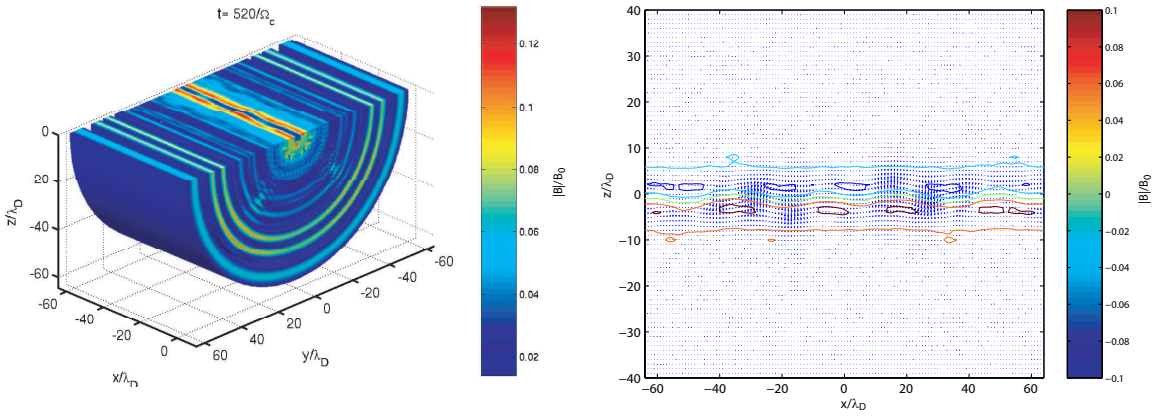

FIG. 1: 3D contour plot of magnetic field strength (left) and the magnetic field profile of the plane $y = 0$ (right) at $t\Omega_{ce} = 520$.

III. RESULTS

First, we study the cylindrical case. Three-dimensional contour plot of magnetic field strength and the magnetic field profile of the plane $y = 0$ at $t\Omega_{ce} = 520$ are shown in Fig. 1. Only a quarter of the whole simulation box is shown in Fig. 1*a*. Electric field E_z is automatically generated by the expansion of magnetic field, and the direction of the Poynting vector is always in the radial direction. EM wave expands to surrounding vacuum region with the speed $\sim c$, carrying particles within its ponderomotive well. Electrons and positrons are also accelerated in the negative and positive z direction respectively, due to $E \times B$ drift, as we expected. Due to the periodic boundary condition, no charge separation occurs in the z direction.

Rayleigh-Taylor instability occurs in the central region ($r < 10\Delta x$). The critical wave number k_x for electron-positron plasma is given by [1]

$$k_x^2 v_0^2 < -g\frac{\rho_0'}{\rho_0}, \tag{3}$$

where $v_0 = -g/\Omega_{ce}$ is the positron centrifugal drift velocity in the x direction, $\rho_0' = d\rho_0/dr$, and $g = v_0^2/r$ is the centrifugal field strength in the radial direction by the magnetic field curvature. The minimum wavelength $\lambda = 2\pi r$ is $\sim 30\Delta x$ on the surface of the initial plasma column, which corresponds to the wavelength in magnetic field profile Fig. 1*b*. Only the center of the column becomes unstable, since ρ_0' rapidly goes to zero toward the edge of magnetic field column.

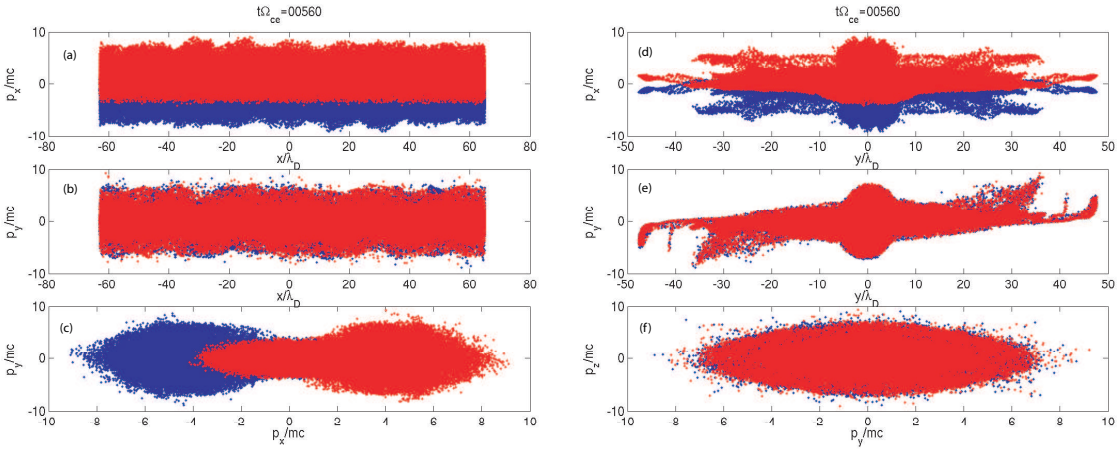

FIG. 2: Phase plots of electrons (blue) and positrons (red) in the cylindrical case at $t\Omega_{ce} = 560$.

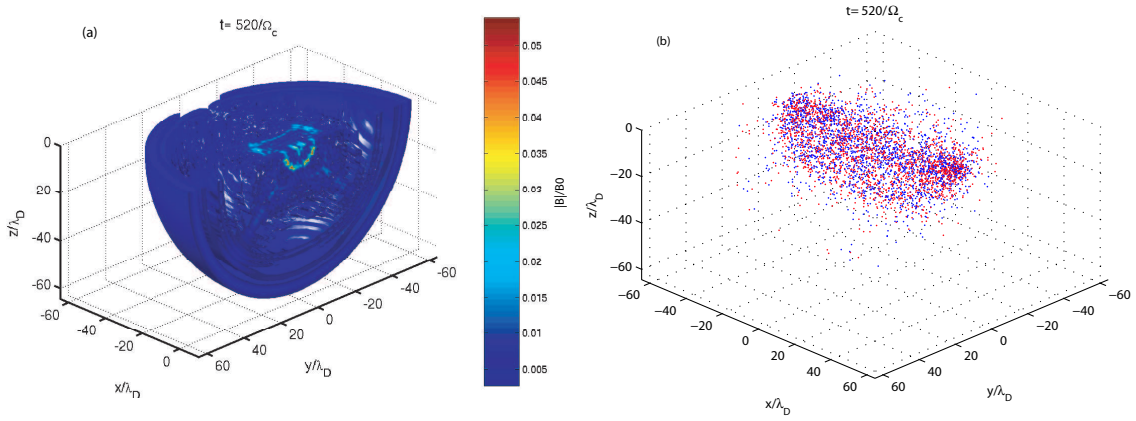

FIG. 3: 3D contour plot of magnetic field strength (a) and the spatial distribution of electrons (blue) and positrons (red) (b) at $t\Omega_{ce} = 520$.

Figure 2 shows phase plots at $t\Omega_c e = 560$. Figure 2a shows that troidal magnetic field B_ϕ create a current in the x direction. Figures 2b and 2c indicates that the most energetic particles are accelerated with $\gamma \sim 10$ in both x and y directions, and slow particles are not accelerated by PFA in y and z. Figures 2d and 2e shows that strong bifurcation occurs in the y direction. The first ponderomotive force well in the front of EM pulse ($y \sim \pm 50\Delta x$) is too weak to hold all the energetic particles, and following ponderomotive wells ($y \sim \pm 40\Delta x$ and $\pm 30\Delta x$) capture such particles slipped out from the first well. Finally, Fig. 2f shows the expansion is uniform in the $y - z$ plane.

Next, we show the results of the torus case. Figure 3a shows the three-dimensional contour

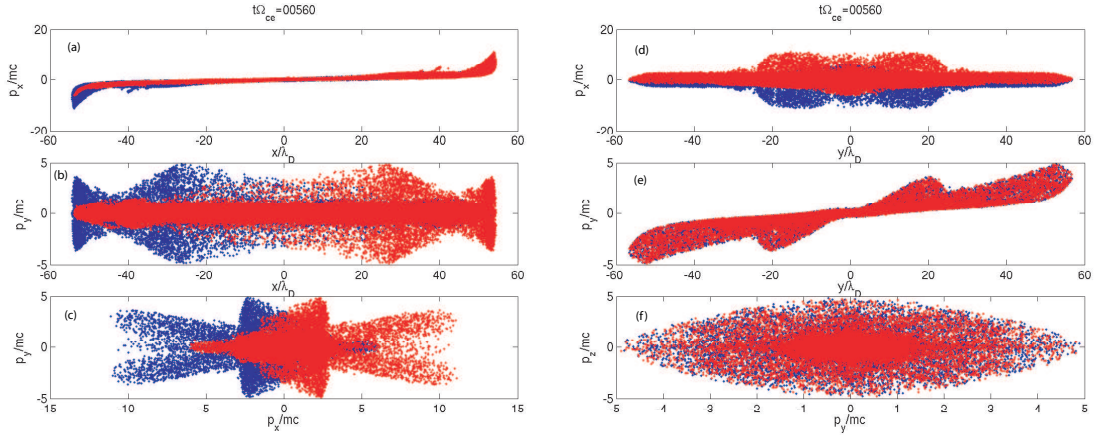

FIG. 4: Phase plots of electrons (blue) and positrons (red) in the cylindrical case at $t\Omega_{ce} = 560$.

plot of magnetic field at $t\Omega_{ce} = 520$. In this case, EM field expands almost spherically. Different from the cylindrical case, the magnetic torus has finite length in the x direction, resulting the charge separation between electrons and positrons. Figure 3b shows the spatial distribution of sample electrons (blue) and positrons (red). Positrons and electrons are tend to move in the positive and negative x direction, respectively, creating electric field in the x direction. Only few particles are captured and accelerated by PFA, since the magnetic field strength drops as $(ct)^{-3}$ in the torus case, whereas $(ct)^{-2}$ in the cylindrical case.

Figure 4 shows phase plots at $t\Omega_c e = 560$. Figure 4a indicates strong acceleration occurs on the edge of torus, creating charge separation. The highest γ factor for the most energetic particles is ~ 10, which is the same order as the cylindrical case. Charge separation may prevent particles from accelerating for long time, but simulation box is too small to see if the acceleration will stop. Figures 4b and 4c shows that the acceleration in the $x-y$ plane is highly non-uniform, and the highest γ in the y direction is almost half of γ in the x direction.

Figures 4d and 4e shows that the acceleration of particles captured in the front of EM pulse ($|y| > 25\Delta x$) is not efficient, and more effective acceleration occurs in the second well ($10\Delta x < |y| < 25\Delta x$). As we mentioned, magnetic field strength drops as r^{-3}, and the first well is too shallow to capture particles in it. The location of the second well corresponds to the propagation of the initial field peak ($r = 2\Delta x$). Finally, Fig. 4f shows the expansion is uniform in the $y - z$ plane.

IV. SUMMARY

We studied 3D PIC simulations of particle acceleration driven by PFA with two different initial magnetic field configurations. Acceleration by PFA is robust in both cases, without showing any instability. The efficiency, however, strongly depends on how strong magnetic field is and how it expands. In the cylindrical case, we observe acceleration of particles in the radial direction as well as the axial direction. Acceleration in the axial direction is due to $E \times B$ force, whereas in the radial direction is by PFA. Without support from external ambient pressure, EM wave expands indefinitely with decaying the field strength proportional to $(ct)^{-2}$. Bifurcation in the phase space occurs because the ponderomotive potential well becomes too shallow to hold particles in it. Rayleigh-Taylor instability occurs at the center, which does not affect the particle acceleration by PFA.

In the torus case, the expansion of magnetic field is spherical rather than cylindrical, and the magnetic field strength decays with $(ct)^{-3}$. As a result, the front potential well is too weak to hold particles, and radial acceleration by PFA is not as efficient as the cylindrical case. Another important difference is the charge separation between electrons and positrons, which may terminate the acceleration in the axial direction.

Our simulation results show that hydrodynamical and/or MHD simulations are not sufficient to understand the acceleration process in collapsar jets. We are planning to run more realistic model to simulate the acceleration and radiation of particles by jets.

Acknowledgments

This research is partially supported by NASA Grant No. NAG5-9223, NSF Grant No. AST0406882, and LLNL contract nos. B528326 and B541027. The authors wish to thank ILSA, LANL, B. Remington and S. Wilks for useful discussions.

---

[1] Chen, F. F.,:Plasma Physics and Controlled Fusion, Vol. 1, Plenum Press, New York(1984)

[2] Berezinskii, V. S., Prilutskii, O. F.: A& A, **175**, 309 (1987)

[3] Kato, Y., Mineshige, S., Shibata, K.: ApJ, **605**, 307 (2004)

[4] Liang, E., Nishimura, K.: Phys. Rev. Lett., **92**, 175005 (2004)

[5] Lynden-Bell, D.: MNRAS, **341**, 1360 (2003)

[6] MacFadyen, A. I., Woosley, S. E.: ApJ, **524**, 262 (1999)

[7] Nagataki, S.: ApJS, **127**, 141 (2000)

[8] Nagataki, S.: ApJS, **551**, 429 (2001)

[9] Nagataki, S.,Kohri, K.,Ando, S., Sato. K.: Astropart. Phys., **18**, 551 (2003)

[10] Noguchi. K., Liang, E., Nishimura, K.: Nuovo Ciment C, **028**, 381 (2005)

[11] Woosley, S. E.: ApJ, **405**, 273 (1993)

[12] Yee, K. S.: IEEE Trans. Antennas Propag., **14**, 302 (1966)